Petrellis *EURASIP Journal on Wireless Communications and Networking* (2016) 2016:122
DOI 10.1186/s13638-016-0619-z

EURASIP Journal on Wireless Communications and Networking

RESEARCH Open Access

Optimal reception of sub-sampled time-domain sparse signals in wired/wireless OFDM transceivers

Nikos Petrellis

Abstract

A time domain sub-sampling technique that can be applied to wired or wireless orthogonal frequency division multiplexing systems is described in this paper. Focus is given on the specific conditions that allow optimal sparse information recovery. The advantage of the proposed method is that it can be implemented with very low complexity hardware, since it is based on deterministic non-iterative operations. A sub-sampling operating mode is used when sparse information is detected by the receiver and can be applied up to 75 % of the time. The power consumed by the various modules can be significantly reduced during the sub-sampling mode. These modules include the analogue/digital converter and the (inverse) Fast Fourier Transform, as well as the buffering memory used by these modules. The signal to noise ratio analysis shows that an optimal signal reception can be achieved if low order quadrature amplitude modulation and Fourier Transform size are used. Full information recovery can be achieved in some cases of wired communication. A bit error rate lower than 10^{-3} is measured, if fewer than 1/16 of the Fourier Transform input symbols are omitted at the receiver. A space-time block code system is also modelled, to test the proposed sub-sampling method in a wireless environment.

Keywords: Analogue digital conversion, Block codes, Fourier Transform, OFDM, Signal sampling

1 Introduction

Fewer samples than the ones required by the Nyquist theorem can be used for signal recovery, if the information exchanged is sparse or compressible. In this case, a sampling rate close to the actual information rate can be used (analogue to information conversion-AIC). The compressive (or compressed) sensing (or sampling) methods, (CS for short) [1] are based on this principle. Several CS methods are referenced in this paper, in order to compare their hardware implementation complexity and efficiency with the proposed method. However, the proposed method is not derived from CS. A large number of resources are required for the hardware implementation of a CS approach, as described for example, in [2, 3]. The CS techniques have been extensively used in the application domain of image processing [4, 5]. It is assumed that the information is concentrated at specific parts of the sparse images like radar spots in [4], or smaller areas in the center of the landscape in [5]. The efficiency of the CS approach used in [4] or [5] depends on these image features. CS can also be used in sensor network applications [6]. In [7], the CS problem model is solved as a Kalman filter. In [8], a video sequence is separated into slowly changing background and sparse foreground. In [9], the proposed algorithm is used for binary linear classification and feature selection in the context of CS.

The orthogonal frequency division multiplexing (OFDM) is used in a diversity of telecommunication standards. Although it offers high data rates, it requires hardware resources with high complexity and power consumption. The information exchanged in OFDM environments is not generally sparse. Most of the proposed CS techniques are used for OFDM channel estimation. A few subcarriers transfer special symbols (pilots) that are expected by the receiver. The rest of the subcarrier frequencies are estimated by interpolation. When CS is employed, the number of pilots can be kept small even in systems with large delay spread and multipaths like multiple-in multiple-out (MIMO) transceivers [10]. The

Correspondence: npetrellis@teilar.gr
Department of Computer Science and Engineering, TEI of Thessaly, Larissa, Greece

most appropriate approach for comparison is [11] where CS is used both for the channel estimation and the data recovery in an OFDM system.

The most computational intensive and power greedy operation in an OFDM environment is the Fast Fourier Transform (FFT). The FFT and the inverse-FFT (IFFT) are performed at the OFDM receiver and transmitter, respectively. The implementation of a discrete Fourier Transform (DFT) with an N-pt FFT requires $O(N \cdot logN)$ steps. If most of the Fourier coefficients of a signal are small or equal to zero, then the output of the DFT is sparse. In this case, compression methods can be applied (JPEG, MPEG, etc). FFTs implemented with fewer than $O(N \cdot logN)$ operations can be found in [12–14]. A MIMO-OFDM cognitive radio is described in [15]. Compressively sensed data are recovered, using fewer hardware resources: a single analogue/digital converter (ADC) and smaller buffer memory. The energy consumed by the ADC in wideband cognitive radio networks where compressed spectrum sensing is used, is examined in [16].

In this paper, an OFDM architecture that can support sub-sampling is proposed. The sub-sampling mode is applied when sparse information exchange (the number of non-zero bits is lower than a threshold) is detected both at the transmitter and the receiver. In this case, several multiplications/additions of the transmitter IFFT and the receiver FFT can be omitted. Moreover, the ADC on the receiver side operates at lower sampling rate. The system returns to the normal operating mode when the exchange of sparse data is terminated. The data sparseness in time domain and some properties of the DFT transform are exploited. Appropriate IFFT input packet structures are employed for the recovery of the exchanged information on the receiver side from fewer samples. The missing samples at the input of the receiver FFT are replaced by others that have already been received. During the time intervals where sparse data exchange takes place, the power consumption of the ADC and the FFT/IFFT, is reduced. Moreover, the dynamic allocation of lower buffering memory is feasible. The FFT/IFFT butterfly outputs are predictable when the input data is sparse. Thus, the speed of these modules can be increased by cancelling several of their operations.

The potential applications of this work include OFDM network infrastructures where sparse information is permanently transmitted, like for example, night surveillance cameras. In this case, simpler ADC and IFFT/FFT implementations with small memory can be used by the OFDM transceivers, in order to support the proposed sub-sampling scheme. However, there are several other ways to save power and reduce complexity in telecommunication systems with permanent sparse data exchange. For example, CS techniques can be applied at the input data in order to reduce the number of subcarriers used. Moreover, customized measurement matrices can be defined, that are based on random DFT matrix row selection. However, the proposed OFDM architecture can be preferably used in general OFDM network infrastructures with fixed number of subcarriers, where sparse data may occasionally be exchanged. It is assumed that the sparse data exchange lasts long enough to apply efficiently the sub-sampling process. The beginning of the sparse data transmission can be detected by a simple counter on the receiver side that checks if the number of trivial values in a segment is higher than a threshold. The end of sparse data transmission can be detected by a higher network layer at the receiver, if an excessive number of errors are detected. This condition can be recognized through checksums/parity bits, or by counting the errors that occur in segments with known value. In this case, the sub-sampling process is forced to terminate and the last data segment may need to be retransmitted. The sparse data can be derived by sensors, surveillance cameras, etc. The original data can be sparsified if they are not inherently sparse, e.g., by setting to 0 the values that are below a specific threshold. The proposed architecture can be used if the successive sample differences are sparse. It can also be used if sparse information in the frequency domain is transmitted over OFDM, like for example the transfer of compressed images. Power can still be saved at the idle intervals between successive sessions. The number of samples, required for the information recovery in the present work, is higher than other signal reconstruction approaches like CS. However, the implementation of the proposed method has extremely lower complexity since it is not based on optimization problems.

The work presented here is an extension of the work presented in [17, 18]. In [17], a single transmitter and receiver with wired communication channel were assumed. An example N-pt IFFT input symbol structure with four pilots and $N = 1024$ symbols was used in both [17, 18]. This structure included padding with 96 symbols at the beginning and 156 at the end. The operations that can be omitted and the memory savings in a specific FFT implementation were discussed in [17]. The simulations were performed in [17] for data sparseness between 0.5 and 4 %. The number of substituted samples ranged between 64 ($N/16$) and 256 ($N/4$). In [18], the sub-sampling method of [17] is introduced for 2×2 wireless MIMO systems that use OFDM with space-time block coding (STBC).

The present work differs from [17, 18] in the following: (a) the number of samples that can be omitted by the sub-sampling process is theoretically extended by 50 % (up to $3N/8$), since additional DFT properties are exploited, (b) the operations of both the IFFT and the FFT that can be deactivated during the sub-sampling mode are specified in detail, (c) a number of new IFFT input packet

structures, that do not depend on the position of the pilots and the guard symbols, are introduced, allowing the use of the proposed sub-sampling method in MIMO systems and (e) the signal to noise ratio (SNR) and signal to interference and noise ratio (SINR) are modelled for wired and wireless communication. The purpose of this SNR/SINR modelling is to determine the contribution of various parameters to the reception error when typical wired and wireless channels are considered.

The sub-sampling method with emphasis on the new techniques proposed in this paper are presented in Section 2. More specifically, the DFT properties exploited to support sub-sampling are discussed in 2.1. Then, a detailed estimation of the parameters that affect the achieved BER and the IFFT/FFT operations that can be omitted, during the sub-sampling mode, are presented in subsections 2.2 and 2.3, respectively. A wireless STBC-OFDM system, with two transmit antennas, is presented in 3.1. In 3.2 a model of the SINR for wireless MIMO systems is discussed. Simulation results and a comparison with other signal reconstruction methods can be found in Section 4.

2 Sub-sampling in OFDM systems for wired communications

2.1 OFDM architecture and sub-sampling method

The binary data stream at the transmitter input of an OFDM system is encoded in order to generate a parity bit stream. These parity bits are used for the error correction on the receiver side (forward error correction - FEC). $Log_2 q$ bits from the interleaved parity/data bit streams are mapped to the corresponding q-order quadrature amplitude modulation (q-QAM) constellation symbols. The N-pt IFFT that follows, accepts N, q-QAM symbols: X_k, $(0 \leq k < N)$ at its input that are arranged in a proper order and generates the time symbols $x_n (0 \leq n < N)$. The target of the IFFT is to perform the frequency division multiplexing by placing various X_k symbols on different orthogonal subcarriers. Different users may transmit on dedicated subcarriers. An optimal spectrum allocation may be performed in cognitive radio (CR) applications. Some special pilot symbols are placed on reserved subcarriers. The receiver is aware of the pilot positions and their values in order to perform channel equalization.

The reverse procedure is followed at the receiver. The symbols (y_n), received by the channel, form the N-pt FFT input. In an Additive White Gaussian Noise (AWGN) channel, $y_n = x_n + z_n$. The symbol z_n stands for the noise that corresponds to the symbol y_n. Although, there are more accurate ways to describe a communication channel, the AWGN is a generally accepted model for wired channels. Moreover, the proposed sub-sampling method does not depend on the selected channel modelling, although this modelling can affect the information recovery error. A different channel model is used for wireless channels. The modification of the proposed sub-sampling method for wireless channels is dictated by the STBC encoding, rather than the used channel model. The output of the FFT is the set of N-symbols: Y_k. An appropriate FEC method (e.g., Viterbi, low density parity check-LDPC, turbo decoder, etc) uses the received parity bits for the correction of as many errors as possible, without the use of packet retransmission.

The sub-sampling method proposed here, takes advantage of the input data sparseness. The position of the non-zero data is not important since the interleaver scatters them throughout the IFFT input. The proportion of the non-zero data affects the error rate at the receiver. Several q-QAM symbols have identical value due to the data sparseness and can be placed at specific positions at the input of the IFFT. The symbols at the output of the receiver FFT are expected to match the transmitter IFFT input symbols, even if a number of samples at the FFT input are replaced by others (sub-sampling) that have already been received. This can be achieved by exploiting certain DFT properties. The sub-sampling can be realized by reducing the ADC sampling rate on the receiver.

The type of FEC encoder adopted at the OFDM transmitter has to be taken into consideration when the proposed sub-sampling method is defined. The type of FEC encoder used affects the parity pattern predictability that is employed in this approach. Moreover, the FEC type also affects the IFFT input symbol structures that can be used. The recursive systematic convolutional (RSC) encoder, described in [17] will be used, since recursive encoders are more effective in correcting errors at the destination. The encoder used is described by the feed forward and feedback polynomials: $1 + D + D^2 + D^3$ and $1 + D + D^2$, respectively. However, similar predictable parity patterns and appropriate IFFT input structures can be defined for non-recursive encoders. The outputs of the RSC encoder used here are the original input data stream (systematic output) and the parity output. The interleaver used in this work, generates q-QAM constellations, either from parity, or data bits only. For this purpose, a small buffer is used at the output of the FEC encoder in order to store $log_2(q)$ bits from each one of the two RSC encoder outputs.

As described in [19], the minimum Trellis decoding diagram for a specific RSC encoder depends on the order of the forward and feedback polynomials. The parity output of the employed RSC encoder remains "0" until the first "1" appears at its input. Then, the 7-bit pattern shown in Fig. 1a is repeated until another "1" appears at the data input. A different 7-bit repeated pattern is generated then at the encoder parity output, until a third "1" appears and so forth. If the input data are sparse and an appropriate interleaving scheme is selected then, the distance between successive 1's can be long. Consequently,

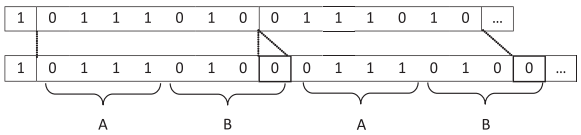

Fig. 1 RSC encoder output. **a** The first 7-bit parity pattern generated from the RSC encoder of [17] after a single "1" at its input (*top row*). **b** the parity patterns padded with "0" bits to form 8-bit parity patterns appropriate for 4-, 16-, and 256-QAM modulation (*bottom row*)

a larger number of identical successive 7-bit patterns will appear at the parity output. This property is exploited in order to place predictable parity QAM symbols at specific positions of the IFFT input, as required by the proposed method. Assume, for example, that identical 128-QAM parity symbols have to be placed at the positions No. 5 and No. $N/2$-5 of the$N$-pt IFFT input. Successive identical parity symbols derived by the 7-bit pattern of Fig. 1a, can be directly placed in these positions. If 256-QAM modulation is used in the OFDM system then, the 7-bit parity can be padded with one "0", as shown in Fig. 1b, to form successive equal 8-bit parity symbols. A 16-QAM modulation is used in most of the case studies of this paper. The padded structure of Fig. 1b can be used again in these cases, to form successive 4-bit parity symbol pairs that are expected to be equal. Different types of FEC encoders described by higher order feedback/feed forward polynomials, non-recursive or non-convolutional ones, etc. can also be considered. They would also generate predictable parity patterns of potentially different lengths when operating on sparse data. Using the appropriate padding, they could have also been exploited in a similar way, as the patterns shown in Fig. 1 that are used here.

The DFT definition used in this paper has the following form:

$$Y_k = \sum_{n=0}^{N-1} y_n w_N^{-kn}, 0 \le k < N-1 \tag{1}$$

where the twiddle factors w_N^r are defined as $w_N^r = e^{2\pi r/N}$. The IDFT is defined as:

$$x_n = \frac{1}{N} \sum_{k=0}^{N-1} X_k w_N^{kn}, 0 \le n < N-1 \tag{2}$$

The sub-sampling method proposed in [17] is based on the following IDFT expressions:

$$x_n = \frac{1}{N} \left(\sum_{k=0,2,\ldots}^{N-2} X_k w_N^{kn} + \sum_{k=1,3,\ldots}^{N/2-1} \left(X_k - X_{k+N/2}\right) w_N^{kn} \right) \tag{3}$$

$$\begin{aligned} x_{n+N/2} &= \frac{1}{N} \sum_{k=0}^{N-1} X_k w_N^{k(n+N/2)} \\ &= \frac{1}{N} \left(\sum_{k=0,2,\ldots}^{N-2} X_k w_N^{kn} - \sum_{k=1,3,\ldots}^{N/2-1} \left(X_k - X_{k+N/2}\right) w_N^{kn} \right) \end{aligned} \tag{4}$$

As can be seen from Eqs. (3) and (4), the IDFT outputs x_n and $x_{n+\frac{N}{2}}$ are equal, only if X_k and $X_{k+\frac{N}{2}}$, with odd k, are identical. This condition is satisfied if all the data X_k, pad and pilot symbols that have been placed in odd k positions have a common value, that will be denoted henceforth as X_c. This can be guaranteed for the majority of the data symbols, since they are derived by sparse data. Using this property, up to half of the symbols (with odd $n > N/2$), at the receiver can be replaced by others ($y_{n-\frac{N}{2}}$). Thus, up to 50 % of the time, the receiver's ADC can operate at the half sampling rate (sub-sampling mode). If R is the number of y_n values, that can be substituted by their counterparts, at distance $N/2$ then, $R \le N/4$. The R value may have to be selected much lower than $N/4$ in order to achieve an acceptable error. This depends on the sparseness level of the input data. The sub-sampling is applied in uniform intervals and therefore, there is no need to define a customized sampling matrix. The sub-sampling mode is extended in this work, using another DFT property, that concerns the x_n with odd n and $n < N/4$. Taking into consideration that $w_N^{n(N/2-k)} = -w_N^{-nk}$, $w_N^{n(N/2+k)} = -w_N^{nk}$ and $w_N^{n(N-k)} = w_N^{-nk}$ then, the x_n can be expressed as:

$$\begin{aligned} x_n = \frac{1}{N} \Bigg(& \sum_{k=1,3,\ldots}^{N/4} \left(X_k w_N^{kn} - X_{N/2-k} w_N^{-kn} \right) \\ & + \sum_{k=1,3,\ldots}^{N/4} \left(-X_{k+N/2} w_N^{kn} + X_{N-k} w_N^{-kn} \right) \\ & + \sum_{k=2,4,\ldots}^{N/2-2} \left(X_k w_N^{kn} + X_{N-k} w_N^{-kn} \right) + X_0 - X_{N/2} \Bigg) = x_{N/2-n} \end{aligned} \tag{5}$$

The IFFT output symbols x_n and $x_{N/2-n}$ are equal if $X_k = X_{\frac{N}{2}-k}$ (with odd k and $k \le N/4$), $X_{k+\frac{N}{2}} = X_{N-k}$ (with odd k and $k \le N/4$) and $X_k = X_{N-k}$, with even k and $0 \le k < N/2$. This can similarly be proven if the value of n is between $N/2$ and N. If the conditions related to Eq. (5) are valid, then the sub-sampling mode can be extended up to 75 % of the time. This can be achieved by replacing (a) the y_n, with odd n between $N/4$ and $N/2$, by the samples $y_{n-\frac{N}{4}}$ and (b) the y_n with odd $n \ge N/2$, by $y_{n-\frac{N}{2}}$. The aforementioned conditions are always true only in the extreme case where all of the input data have the same trivial value (e.g., "0"). However, if the input data

are sparse, these conditions are still valid for most of the k values. The few cases where the data are non-trivial make the conditions described above invalid. These few cases are responsible for the sub-sampling error. The FEC method used can reduce the effect of this error, since it can be viewed as an additional noise source. The new IFFT input packet structure shown in Fig. 2 can be used in order to apply the extended sub-sampling mode. The data symbols (most of them are equal to X_c) have been placed at the even positions.

The first 4-bits (denoted as Parity A) and the last 4-bits (Parity B) of the padded 8-bit parity patterns shown in Fig. 1b, have been placed as follows: the first Parity A, B pair is placed at the positions 1 and 3, respectively, the second A, B pair at the positions $N/2-1$ and $N/2-3$, the third, at the positions 5 and 7, the fourth at $N/2-5$ and $N/2-7$, and so forth. After all the odd positions below $N/2$ have been filled with parity patterns A or B then, the odd positions between $N/2$ and $N-1$ are filled in a similar way. Had successive parity symbols been placed at the odd positions starting from the position 1 towards the position $N-1$, then the conditions related to Eq. (5) would not hold in most cases. This is owed to the fact that the 4-bit Parity A (or B) patterns of the initial padded 8-bit pairs, are probably not equal to the Parity A (or B) patterns of the last pairs in the IFFT input packet. The pilot and padding symbols have not been shown in Fig. 2 but they can be placed in the even positions instead of data symbols if they are selected to be equal to X_c. Alternatively, pairs of padding symbols or pilots, with equal value (potentially different than X_c), can be placed in symmetric odd parity positions around $N/4$, or around $3N/4$. It has to be stressed that in this approach, there are many more options than [17], concerning the allowed positions and values of the padding and the pilot symbols. If the predictable parity patterns consisted of more than two QAM symbols, they would have to be spread appropriately to fulfil the conditions related to the Eqs. (3)–(5).

2.2 The Sub-sampling effect to the SNR

A wired communication between the OFDM transmitter and receiver is assumed and the channel noise is modelled as AWGN in this section. The distortion posed by the sub-sampling operating mode and the quantization noise of the IFFT/FFT operations and the ADC, are considered as noise sources, additional to the z_n. The signal to noise ratio (SNR_{AWGN}) in this type of communication can be defined as the ratio of the signal power P_{SIG}, to the sum of the AWGN noise power on all X_k symbols (σ^2_{noise}), the sub-sampling (P_{SS}) and the quantization (P_Q) error due to the finite system resolution:

$$SNR_{AWGN} = \frac{P_{SIG}}{P_{SS} + P_Q + \sigma^2_{noise}} \tag{6}$$

Equation (6) above is used to determine how the various sub-sampling parameters affect the error on the receiver side, rather than the estimation of an exact SNR value. In this sense, different channel models with potentially higher precision could have also been employed. In the previous section, it was initially assumed that $X_c = X_k = X_{k+N/2}$ for odd k positions, since they were derived from sparse input data. However, this condition is not valid for all the k values since, the input data bits are sparse but they are not all zero. The square error that corresponds to the inequality of X_k with $X_{k+N/2}$ is

$$\begin{aligned}\varepsilon^2_{SS}(k) &= \left|X_k w_N^{kn} + X_{k+N/2} w_N^{(k+N/2)n}\right|^2 = \left|X_k w_N^{kn} - X_{k+N/2} w_N^{kn}\right|^2 \\ &= |X_k|^2 + \left|X_{k+N/2}\right|^2 - X_k X^*_{k+N/2} - X^*_k X_{k+N/2}\end{aligned} \tag{7}$$

If $X_k = \alpha + \beta j$, $X_{k+N/2} = \gamma + \delta j$, then the error ε_{ss} can be generally expressed as: $\varepsilon^2_{ss} = (\alpha-\gamma)^2 + (\beta-\delta)^2$. The maximum absolute real or imaginary dimension of the q-QAM modulation used, is $d = \left|\sqrt{q}\right| - 1$. The maximum error caused by a pair of unequal X_k and $X_{k+N/2}$ values is

$$max\left(\varepsilon^2_{SS}\right) = (\alpha-\gamma)^2 + (\beta-\delta)^2 = 8d^2 \tag{8}$$

The average absolute ε_{sa} for a single X_k and $X_{k+N/2}$ pair is: $\varepsilon_{sa} = \sqrt{2}d$. The probability of a q-QAM symbol (consisting of $log_2(q)$ bits) to be different than X_c, is $S \cdot log_2(q)$, where S is the sparseness level defined as the ratio of the non-zero bits to the total number of data bits. The average ε_{sa} error can appear up to $R \leq N/4$ times in the estimation of a single IFFT output symbol x_n. The power P_{SS} of the sub-sampling error on the receiver side for a single y_n symbols is

$$P_{SS} = (R \cdot S\sqrt{2}d \cdot log(q))^2 \tag{9}$$

The truncation or quantization noise in FIR filters, FFTs, etc is described in [20]. The result of a

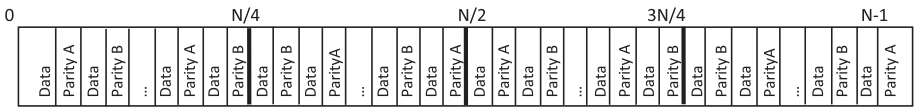

Fig. 2 IFFT input. An appropriate placement of data and parity QAM symbols at the input of the IFFT in order to apply the extended sub-sampling mode

multiplication between two n_b bit numbers requires $2n_b$ bits. If the result has to fit in n_b bits, then the rest of the n_b bits have to be truncated. The round-off error will be a value between $-\frac{2^{-(n_b-1)}}{2}$ and $\frac{2^{-(n_b-1)}}{2}$. The distance between these limits is $d_s = 2^{-(n_b-1)}$. The parameter d_s, represents the minimum difference that can be discriminated between the quantized real numbers. The error probability is assumed to be uniform $(1/d_s)$ between $-d_s/2$ and $d_s/2$. The variance of the error is then estimated as: $\frac{d_s^2}{12}$. Although the quantization noise power in all real and imaginary parts of the DFT outputs is estimated in [20] as

$$P_Q = N\frac{d_s^2}{12} \tag{10}$$

this P_Q noise is reduced to [20]

$$P_Q \leq \frac{d_s^2}{6}(log_2 N - 2) \tag{11}$$

in the real and imaginary parts of all FFT outputs. The upper limit of the relation (11) corresponds to the classic FFT implementation by Cooley and Turkey [21]. The number of multiplications is reduced to $O(log_2 N)$ in [21], from $O(N)$ that were required in the DFT definition of Eq. (1). Modern FFT implementations can further reduce the required number of multiplications below this limit leading to the relation (11), as described in [20]. In [22], time-domain sine-wave peak amplitude characteristics are estimated based on FFT data. Although the scalloping loss characteristics of the FFT degrade the accuracy, the author of [22] presents multiplier-free methods that show a scalloping error as low as 0.0113 dB.

Equations (6), (9), and (11), show that a better SNR can be achieved for small values of R, S, q (d is also proportional to the square root of q), as well as N. The quantization noise is also reduced in low order q-QAM modulations. These parameters can be related directly to the bit or symbol error rate shown by this system using the complementary error function (*erfc*) as described, e.g., in [23]. There are different versions of these relations, depending on the QAM modulation order q and the QAM coding used (e.g., grey coding). However, it can be generally stated that the probability of a symbol error is proportional to $Q(c \cdot \sqrt{SNR_{AWGN}})$, where c is a constant depending on the QAM order q. For example, the probability of symbol error in 4-QAM and 16-QAM is approximately $2Q(\sqrt{2 \cdot SNR_{AWGN}})$ and $3Q(\sqrt{4 \cdot SNR_{AWGN}/5})$, respectively. The Q function is defined as: $Q(x) = \frac{1}{2}erfc\left(\frac{x}{\sqrt{2}}\right) = \frac{1}{2\sqrt{2}}\int_0^{\frac{x^2}{2}} \frac{e^{-t}}{\sqrt{t}}dt$. The erfc function returns a value between 0 and 2. Consequently, the Q function is between 0 and 1. The probability of symbol error tends to 0 as SNR_{AWGN} is increased. However, the sub-sampling error (P_{SS} in Eq. (6)) dominates over the channel noise in this case. Thus, the increase of the overall SNR_{AWGN} is prevented, even if the signal power P_{SIG} gets much higher than the additive noise: σ^2_{noise}. An error floor appears when the value of one or more of the parameters R, S, q, N is high.

2.3 FFT/IFFT implementation issues

A radix-2 N-pt FFT is performed by combining a pair of $N/2$-pt FFTs. The first FFT accepts as input the odd positioned inputs of the N-pt FFT and the second one the inputs from the even positions. The $N/2$-pt FFTs can be recursively implemented by pairs of $N/4$-pt FFTs and so forth until 2-pt FFTs are defined. In this way, the N^2 operations required by the N-pt DFT are reduced to $N \cdot log_2 N$ [21]. The inputs in the FFT sub-blocks are bit reversed while the outputs are in normal order. The implementation of an N-point FFT using two $N/2$-pt FFTs is shown in Fig. 3a. If the number of substituted samples on the receiver side is $R = N/4$, then all the input pairs of the $N/2$-pt, FFT-B with distance $N/4$, are equal. Thus, half of the $N/2$-pt FFT-B output values will be zero, as proved by the Eq. (12) below. The zero outputs of FFT-B in Fig. 3a, are indicated with dashed arrows and the corresponding operations can be omitted. The $N/2$-pt FFTs can be flattened to lower order FFTs in order to apply recursively this property. The fraction of the multiplications and additions that can be omitted if $R = N/4$, is 3/8. If the number of substituted samples R is lower than $N/4$ then, a smaller

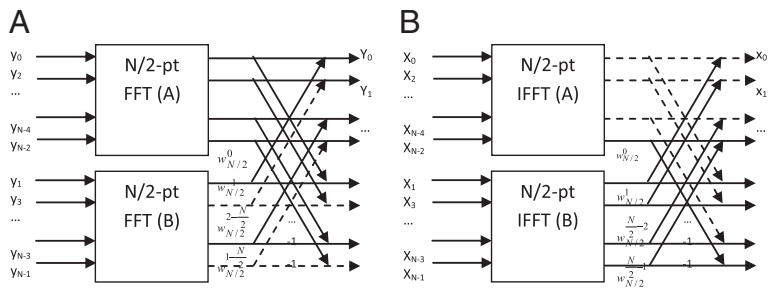

Fig. 3 FFT operations. **a** FFT and **b** IFFT implementation

number of FFT operations can be omitted. For example, if $R = N/8$ then, 1/8 of the additions and multiplications can be discarded.

$$Y_k = \sum_{n=0}^{N/2-1} y_n w_N^{-kn} + \sum_{n=0}^{N/2-1} y_{n+\frac{N}{2}} w_N^{-k(n+N/2)} = \sum_{n=0}^{N/2-1} y_n w_N^{-kn} + (-1)^k \sum_{n=0}^{N/2-1} y_n w_N^{-kn} \quad (12)$$

Figure 3b shows how an N-pt IFFT can be implemented on the transmitter. For example, the data samples X_k (most of them are equal to X_c) can be placed at the even positions of the IFFT input as shown in Fig. 2. Then, only the No. 0 output of the N/2-pt IFFT-A is equal to X_c and the rest of the outputs are 0, as shown by Eq. (13) below. If the IFFT input packet structure of [17] was used, the data symbols should have been placed at the odd positions of the IFFT input. The IFFT-B would have zero outputs in this case.

$$x_n = \frac{1}{N} \sum_{k=0}^{N-1} X_k w_N^{kn} = X_c \frac{1}{N} \sum_{k=0}^{N-1} w_N^{kn} = 0, n \neq 0 \quad (13)$$

The IFFT sub-blocks that can be turned off in the sub-sampling operating mode, can have a size of up to $N/2$. Of course, a small error overhead is posed since some X_k symbols are not equal to X_c. A lower error can be achieved if smaller IFFT sub-blocks are deactivated. Deactivating FFT sub-blocks at the receiver affects more the BER than the deactivation of IFFT sub-blocks. This is due to the fact that the deactivation of larger FFT blocks than those corresponding to the selected R value leads to information loss since FFT blocks with non-identical inputs are turned off. On the other hand, the size of the IFFT block that can be deactivated depends only on the sparseness level of the input data. It is not affected by the number of substituted samples R at the receiver. The deactivation of IFFT operations is based on the assumption that most of the data X_k symbols have the same value X_c.

3 Sub-sampling in STBC-OFDM

3.1 Sub-Sampling in an STBC-OFDM system with two transmit antennas

In this section, the extension of the proposed sub-sampling method in an STBC-OFDM environment is described, in order to demonstrate how it could be employed by a MIMO telecommunication system. Information reconstruction in MIMO-OFDM cognitive radio (CR) is described in [15] using compressive sensing techniques. However, this approach is different compared to the one presented here: CR radios target to the efficient spectrum utilization when several subcarriers are unused by the licensed users. Unlicensed transceivers can exploit dynamically the bandwidth gaps left by these licensed users. The purpose of the proposed method is to reduce the power of the receiver when sparse information is exchanged by the active users, whether they are licensed or unlicensed CR ones.

An STBC-OFDM environment with N_T transmit and one receive antenna is shown in Fig. 4. Alamouti described in [24] an encoding that takes advantage of antenna diversity. In Fig. 4, the generated QAM symbols are arranged in a matrix with N_S columns. The N_S stands for the number of symbols used in a single STBC encoding. The N_S, consecutive QAM symbols form the matrix X_{STBC} with size $N_T \times N_L$, where N_L depends on the N_T. The simplest case of an STBC encoding with two transmit antennas is considered in this paper, to demonstrate how the proposed sub-sampling scheme can be applied to wireless MIMO environments. The STBC encoding uses $N_S = 2$ consecutive QAM symbols X_1 and X_2 in the 2×2, X_{STBC} matrix defined in (14).

$$X_{STBC} = \begin{bmatrix} X_1 & -X_2^* \\ X_2 & X_1^* \end{bmatrix} \quad (14)$$

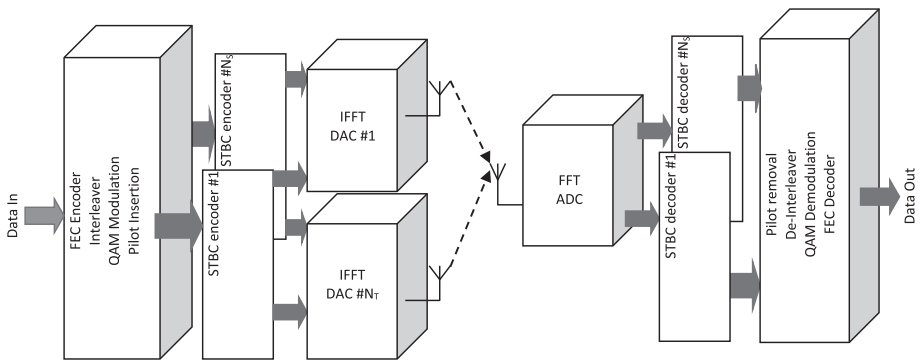

Fig. 4 STBC-OFDM topology. STBC-OFDM telecommunication system with N_T transmit and one receive antenna

If X_{STBC}^H is the Hermitian of X_{STBC}, (*) is the conjugate of a symbol and I_2 is the 2×2 identity matrix:

$$X_{STBC}X_{STBC}^H = \frac{1}{|X_1|^2 + |X_2|^2} I_2 \tag{15}$$

Each transmit antenna will sequentially send the N_L, QAM symbols of each X_{STBC} matrix row. The channel coefficients h_1 and h_2 correspond to the paths between the two transmit antennas and the receiver one. They are assumed to be time invariant throughout the transmission of a single X_{STBC} row. The received symbols Y_1 and Y_2 that correspond to an X_{STBC} row, can be expressed as

$$\begin{array}{l} Y_1 = h_1X_1 + h_2X_2 + Z_1 \\ Y_2 = -h_1X_2^* + h_2X_1^* + Z_2 \end{array} \Rightarrow$$
$$\left[\begin{array}{c} Y_1 \\ Y_2^* \end{array}\right] = \left[\begin{array}{cc} h_1 & h_2 \\ h_2^* & -h_1^* \end{array}\right]\left[\begin{array}{c} X_1 \\ X_2 \end{array}\right] + \left[\begin{array}{c} Z_1 \\ Z_2^* \end{array}\right] \Rightarrow Y = HX + Z \tag{16}$$

where Z_1 and Z_2 is the additive noise corresponding to Y_1 and Y_2, respectively. If h_1 and h_2 are known at the receiver (e.g., through their estimation when X_1 and X_2 are pilot symbols), the following calculation can be performed:

$$\begin{array}{l} \widetilde{Y} = H^H Y = \left(|h_1|^2 + |h_2|^2\right) X + \widetilde{Z} \Rightarrow \\ X = \dfrac{1}{|h_1|^2 + |h_2|^2}\left(\widetilde{Y} - \widetilde{Z}\right) \end{array} \tag{17}$$

The noise factor $\widetilde{Z} = H^H Z$ can be ignored on the receiver. The approximation $\widetilde{X}$ derived by Eq. (17) when $\widetilde{Z}$ is eliminated, can be used and its $\widetilde{X_1}$ and $\widetilde{X_2}$ components can be mapped to QAM symbols through their minimum distance. The rows of the XSTBC matrix are used as input to the N-pt IFFT of Fig. 3. The N of the y_n symbols received by the single antenna form the input to the FFT that generates the Y_k symbols used in Eqs. (16) and (17).

The IFFT input packet structure that is necessary for the sub-sampling in an OFDM environment requires sparse data QAM symbols to be placed either only in odd positions ([17]), or only in even positions as in Fig. 2. In the STBC-OFDM environment with two transmit antennas, the received sample y_n is a combination of the symbols y_n^A and y_n^B arrived from the two transmit antennas A and B. Let h_n^A, h_n^B be the channel coefficients (they can be used to model Rayleigh or Rician fading) that correspond to the paths from the transmit antennas A and B to the single receive antenna. If z_n' is the total noise corresponding to the received symbol y_n, then:

$$y_n = y_n^A + y_n^B = h_n^A x_n^A + h_n^B x_n^B + z_n' \tag{18}$$

If the y_n and $y_{n+\frac{N}{2}}$ are estimated by Eq. (18) and the IDFT definition of Eq. (2) and the IFFT input packet structure of [17] is used, then these symbols are not equal even if $h_n^A = h_{n+\frac{N}{2}}^A = h^A$ and $h_n^B = h_{n+\frac{N}{2}}^B = h^B$ (time invariant channel coefficients) and the noise is ignored. Specifically,

$$y_n = \frac{w_N^{kn}}{N}\left(\sum_{k=0,2}^{N-2}\left(h_n^A X_k^A + h_n^B X_k^B\right) + \right.$$
$$\left. + \sum_{k=1}^{\frac{N}{2}-1}\left(h_n^A\left(X_k^A - X_{k+\frac{N}{2}}^A\right) + h_n^B\left(X_k^B - X_{k+\frac{N}{2}}^B\right)\right)\right) \tag{19}$$

$$y_{n+\frac{N}{2}} = \frac{w_N^{kn}}{N}\left(\sum_{k=0,2}^{N-2}\left(h_n^A X_k^A + h_n^B X_k^B\right) - \right.$$
$$\left. - \sum_{k=1}^{\frac{N}{2}-1}\left(h_n^A\left(X_k^A - X_{k+\frac{N}{2}}^A\right) + h_n^B\left(X_k^B - X_{k+\frac{N}{2}}^B\right)\right)\right) \tag{20}$$

As can be seen from Eqs. (19) and (20), although the sums of the even-positioned X_k symbols in both y_n and $y_{n+\frac{N}{2}}$ are equal, the sums of the symbols in the odd positions have an opposite sign. The only way to have equal y_n and $y_{n+\frac{N}{2}}$ is to have both $X_k^A = X_{k+\frac{N}{2}}^A$ and $X_k^B = X_{k+\frac{N}{2}}^B$ for all the odd k's. This cannot be guaranteed with the IFFT packet structure described in [17] nor with the one described in Fig. 2 in this work. However, if two parallel Fig. 2 symbol structures are used at the input of the transmitter STBC encoder then, the proposed sub-sampling schemes can be applied. This is because the symbols X_1 and X_2 in the matrix X_{STBC}, will be both equal data or parity symbols. More specifically, if an X_{STBC} matrix is derived from data symbols X_c, the odd positions of IFFT input in the transmitter A will be of the form $X_k^A = X_{k+\frac{N}{2}}^A = -X_c^*$. Similarly for the IFFT of the transmitter B: $X_k^B = X_{k+\frac{N}{2}}^B = X_c^*$. If the X_{STBC} matrix is derived from parity symbols A (X_{ParA}), the odd positions of the IFFT input of the transmitter A, will be $X_k^A = X_{k+\frac{N}{2}}^A = -X_{ParA}^*$ and the ones at the IFFT of the transmitter B: $X_k^B = X_{k+\frac{N}{2}}^B = X_{ParA}^*$. If the X_{STBC} matrix is derived from parity symbols B (X_{ParB}), we will have again: $X_k^A = X_{k+\frac{N}{2}}^A = -X_{ParB}^*$ (odd positions at the IFFT input of the transmitter A) and $X_k^B = X_{k+\frac{N}{2}}^B = X_{ParB}^*$(transmitter B). These conditions hold with high probability if the data sparseness is high and the predictable parity patterns A and B of Fig. 1 are spread appropriately as described in Section 2.1. In this case: X_k^B (or X_k^A) and $X_{k+\frac{N}{2}}^B$ (or $X_{k+\frac{N}{2}}^A$) are derived from successive parity patterns and are expected to be equal. The second sums of both Eqs. (19) and (20) are zero and $y_n = y_{n+\frac{N}{2}}$.

The extended sub-sampling scheme described by Eq. (5) in Section 2.1 cannot be applied successfully to the IFFT input structure described above because the following conditions do not hold: $X_k = X_{\frac{N}{2}-k}$ (with odd k and $k \leq N/4$), $X_{k+\frac{N}{2}} = X_{N-k}$ (with odd k and $k \leq N/4$). However, alternative IFFT input packet structures can be defined that will also fulfil these conditions. The selection of IFFT input structures appropriate for the extended sub-sampling scheme is part of our future work.

3.2 Effect of sub-sampling to the wireless MIMO channel SINR

Several SINR models for MIMO systems have been proposed in the literature for specific applications [16, 25]. A worst case SINR modelling is briefly presented in this section for the topology of Fig. 5. The purpose of the following SINR model is to define the effect of the sub-sampling, multipath, inter-symbol interference and quantization noise, in the reception error of a general MIMO system (not necessarily STBC). Figure 5, shows how the signal of multiple (M_T) transmitters arrives at the receiver while the useful communication is between transmitter Tx0 and receiver Rx0. The signal of the rest of the transmitters is considered as interference. The symbol y_n at the receiver Rx0 that corresponds to the symbol $x_0(n)$ transmitted by Tx0 at time n, is expressed as follows:

$$y_n = x_0(n)h_0(0) + \sum_{t=1}^{M_T-1} x_t(n)h_t(0) + \sum_{l=1}^{L-1}\sum_{t=0}^{M_T-1} x_t(n-l)h_t(l) + z_n \tag{21}$$

where the interference of the other transmitters, the inter-symbol interference (ISI) and white Gaussian noise z_n are taken into consideration. The number of interfering transmitters is $M_T - 1$. The useful information is represented by the first term in the addition of Eq. (21). The second term corresponds to the line of sight (LOS) interference

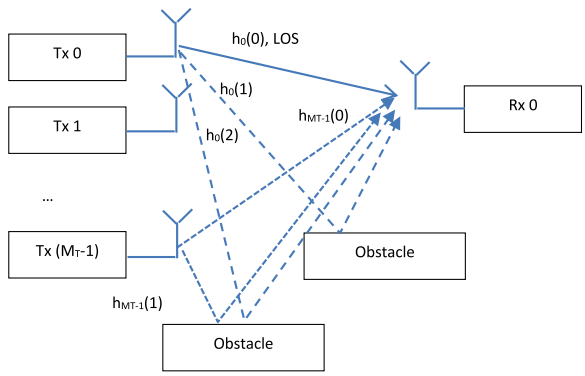

Fig. 5 The wireless channel. A channel model that takes into consideration fading and multipaths

of the other transmitters. The third term models the ISI from the non-LOS (NLOS) paths of both the transmitter Tx0 and the rest of the transmitters. The maximum number of paths, a transmitter signal follows in order to reach the receiver is L.

The N of the y_n symbols are used as input to the FFT that generates the N, symbols Y_k on the receiver side. These Y_k symbols are used to estimate the original X_k, q-QAM transmitted symbols:

$$\begin{aligned} Y_k &= \sum_{n=0}^{N-1}(x_0(n)h_0(0) + \sum_{t=1}^{M_T-1} x_t(n)h_t(0) \\ &\quad + \sum_{l=1}^{L-1}\sum_{t=0}^{M_T-1} x_t(n-l)h_t(l) + z_n)w_N^{-nk} \\ &= \sum_{n=0}^{N-1} x_0(n)h_0(0)w_N^{-nk} + \sum_{n=0}^{N-1}\sum_{t=1}^{M_T-1} x_t(n)h_t(0)w_N^{-nk} \\ &\quad + \sum_{n=0}^{N-1}\sum_{l=1}^{L-1}\sum_{t=0}^{M_T-1} x_t(n-l)h_t(l)w_N^{-nk} + \sum_{n=0}^{N-1} z_n w_N^{-nk} \end{aligned} \tag{22}$$

The factor $h_t(l)$ represents the channel coefficient for the signal of the transmitter t that arrives to the receiver from path l. The symbol $x_t(n)$ represents the IDFT output from the same transmitter. Each term of Eq. (22) is treated separately in order to estimate its power. The signal to interference, noise and distortion ratio (SINDR) that takes into consideration the digitization and the sub-sampling error can be expressed as:

$$SINDR = \frac{P_{SIG}}{P_{IF} + P_{ISI} + P_{SS} + P_Q + \sigma_n^2} \tag{23}$$

where an estimation of P_Q similar to the relation (11) can be used for the estimation of one Y_k symbol by the receiver FFT. The power of the signal (P_{SIG}), the interfering transmitters (P_{IF}) and the ISI (P_{ISI}) can be estimated by the Eq. (22) as follows:

$$P_{SIG} = \left|Y_k^{SIG}\right|^2 = |h_0(0)|^2 \left|X_{0,k}\right|^2 \tag{24}$$

$$P_{IF} = \left\|Y_k^{IF}\right\|^2 = \left\|\overline{h}'(0)\overline{X}'(k)\right\|^2 = \left\|\overline{h}'(0)\right\|^2 \left\|\overline{X}'(k)\right\|^2 \tag{25}$$

$$P_{ISI} = \left\|Y_k^{ISI}\right\|^2 = \left\|\overline{H}'(k)\right\|^2 \left\|\overline{X}_k\right\|^2 \tag{26}$$

where Y_k^{SIG}, Y_k^{IF} and Y_k^{ISI} are the first, second and third sum terms of Eq. (22), respectively. The vectors $\bar{h}'(0)$ and $\bar{X}'(k)$ in Eq. (26) are formed by the factors $h_t(0)$ and $X_{t,k}$ (the X_k symbol sent by the transmitter t) respectively, for

$t \neq 0$. The $H_t^{'}(k)$ is the DFT of the $L-1$ channel coefficients $h_t(1), h_t(2),$ Ě, $h_t(L-1)$. The vectors $\overline{X}_k$ and $\overline{H'}(k)$ are formed by the $X_{t,k}$ and $H_t^{'}(k)$, respectively, for every transmitter t.

Equations (9) and (11) defined the contribution of the sub-sampling and the digitization error in one y_n symbol. The Sum Y_k^{SS} of the sub-sampling errors of all the y_n symbols used in the estimation of Y_k, is:

$$\begin{aligned} Y_k^{SS} &= \sum_{n=0}^{N-1} \varepsilon_{sa}(n) w_N^{-nk} \\ &= \sum_{n=0}^{N-1} RS\sqrt{2}dlog_2(q) w_N^{-nk} = RNS\sqrt{2}dlog_2(q) \end{aligned} \tag{27}$$

The sub-sampling error is concentrated in Y_0, since the sum of the twiddles in Eq. (27) is 0, if $k \neq 0$ and N, if $k = 0$. The power contribution P_{SS} of the sub-sampling error is

$$\begin{aligned} P_{SS} &= \left\| Y_k^{SS} \right\|^2 = \left| Y_0^{SS} \right|^2 + \left| Y_1^{SS} \right|^2 + \ldots + \left| Y_{N-1}^{SS} \right|^2 \\ &= \left| Y_0^{SS} \right|^2 = 2R^2N^2S^2d^2log_2^2(q) \end{aligned} \tag{28}$$

No SNR improvement technique was exploited in the analysis above, like for example, multipath diversity in code division multiple access (CDMA). Moreover, the signal and noise power components used in Eq. (23), were not normalized. Similarly to the case of a wired channel, a higher SINDR can be achieved with low R, S, N values and low-order QAM modulation as will be confirmed by the following simulations.

4 Simulation results and case studies

4.1 Simulation results of the sub-sampling method for wired and wireless telecommunication systems

The verification of the proposed sub-sampling method in wired OFDM telecommunications is performed using the environment described in Section 2.1 with a single transmitter/receiver and AWGN channel noise. The Viterbi decoding algorithm was used in this paper. A FEC method based on Reed Solomon codes has also been tested with the setup described in [17] and compared to Viterbi, but their behaviour was similar. However, the same BER can be achieved at lower SNR (4dB in some cases) with FEC decoding, compared to the case when FEC decoding is not used at all. The SNR analysis of Sections 2.2 and 3.2 showed that a higher SNR can be achieved if the data sparseness is high (i.e., the parameter S is low), the number of substituted samples R, is low, the FFT/IFFT size N, is small and low order q-QAM modulation is used. Figure 6 shows the simulation of a wired OFDM system with 4-QAM modulation (QPSK) and $N = 1024$ for various

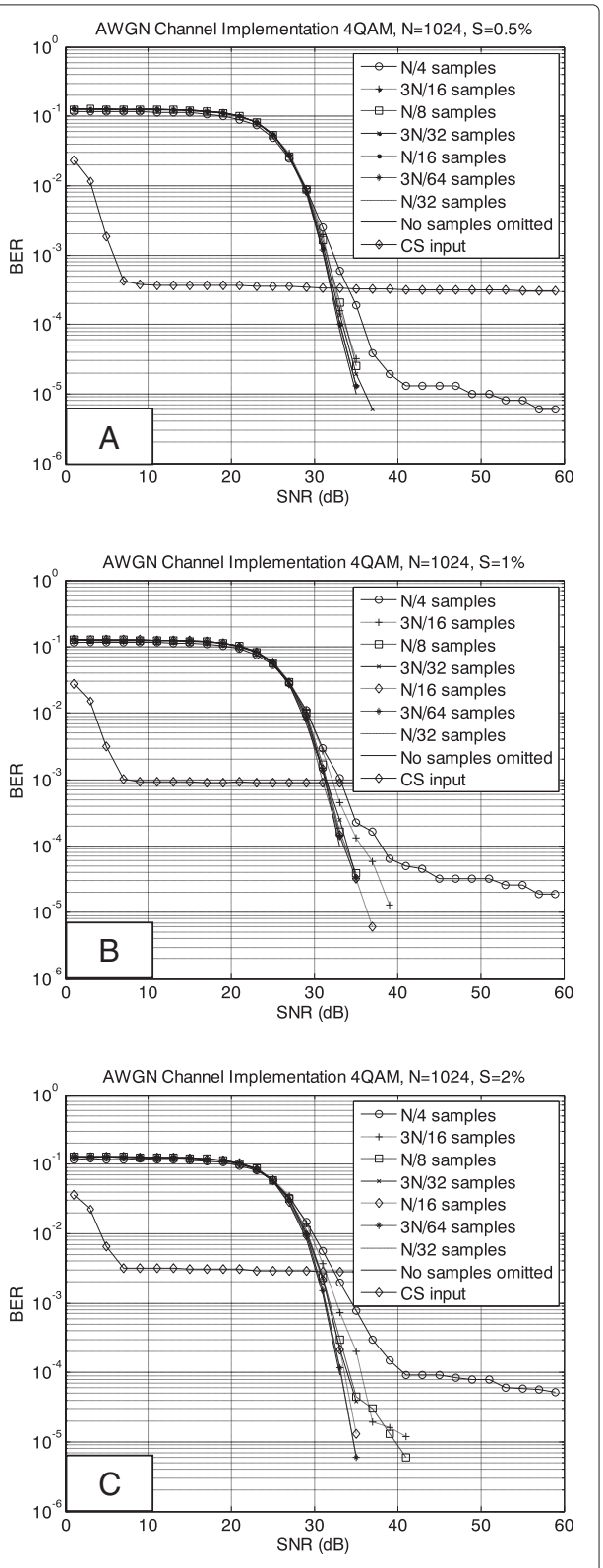

Fig. 6 Simulation Results. Wired OFDM with AWGN channel, $N = 1024$ and 4-QAM modulation. **a** Sparseness level $S = 0.5\,\%$, **b** $S = 1\,\%$, **c** $S = 2\,\%$

sparseness levels S ($S = 0.5\,\%$, $1\,\%$, or $2\,\%$) and number of substituted samples R. The values $R = 3N/16$, $R = 3N/32$ and $R = 3N/64$ correspond to the extended sub-sampling that is performed 75 % of the time while the rest of the R values correspond to the older sub-sampling mode performed 50 % of the time [17]. The IFFT input packet structure used is the one displayed in Fig. 2.

Two reference curves are included in the simulations presented in Fig. 6 corresponding to (a) no sample replacement ($R = 0$) and (b) the use of CS techniques i n time domain at the input of the OFDM environment. In (b), the same input data used with the rest of the case studies are CS compressed, in order to use fewer carriers. For fair comparison, the number of carriers used in (b) is $3N/4$ corresponding to the higher number of omitted samples examined with the proposed sub-sampling scheme. These carriers are loaded with the $3N/4$ measurements generated by the applied CS technique. For this reason, the digitization of the $3N/4$ measurements is performed with the same number of bits that correspond to the QAM modulation used (4-QAM, i.e., 2 bits for Fig. 6). The low resolution used in the digitization of the CS measurements is responsible for the error floor of the curves in Fig. 6 that correspond to the CS input. The decoded bit stream at the OFDM receiver is converted to an analogue value that represents the measurements that had been digitized at the transmitter. Then, the CS optimization target is solved to recover the initial data.

The SNR on the horizontal axis of Fig. 6, reflects only the level of the AWGN noise and does not take into account the sub-sampling and quantization error. The effect of these error sources is demonstrated by the achieved BER. As can be seen from the simulations of Fig. 6, a signal reception with no errors is possible in all cases but the one for $R = N/4$. A very low error floor appears in this case between 10^{-5} (when $S = 0.5\,\%$) and 10^{-4} (when $S = 2\,\%$). In all other cases a correct signal reception is possible when the additive channel noise SNR is between 30 and 40 dB.

In Fig. 7, the same simulations are repeated for 16-QAM modulation and $N = 256$. As can be seen in this figure, the BER is worse than Fig. 6, due to the higher order QAM modulation used despite the lower N size. More specifically, a correct signal reception is possible when $R < 3N/32$ (in the case of $S = 0.5\,\%$). The error floor when $R = N/8$ and $R = 3N/32$, is below 10^{-3}. When $S = 2\,\%$, an error floor appears in all cases. Nevertheless, in most of the cases it is quite low. The CS input reference curves have a lower (or no) error floor in Fig. 7 compared to Fig. 6, due to the digitization with higher resolution of the CS measurements (4-bits for 16-QAM modulation). More simulation results can be found in [17] where different combinations of S, R, N and q are examined for the case of wired OFDM systems and AWGN channel.

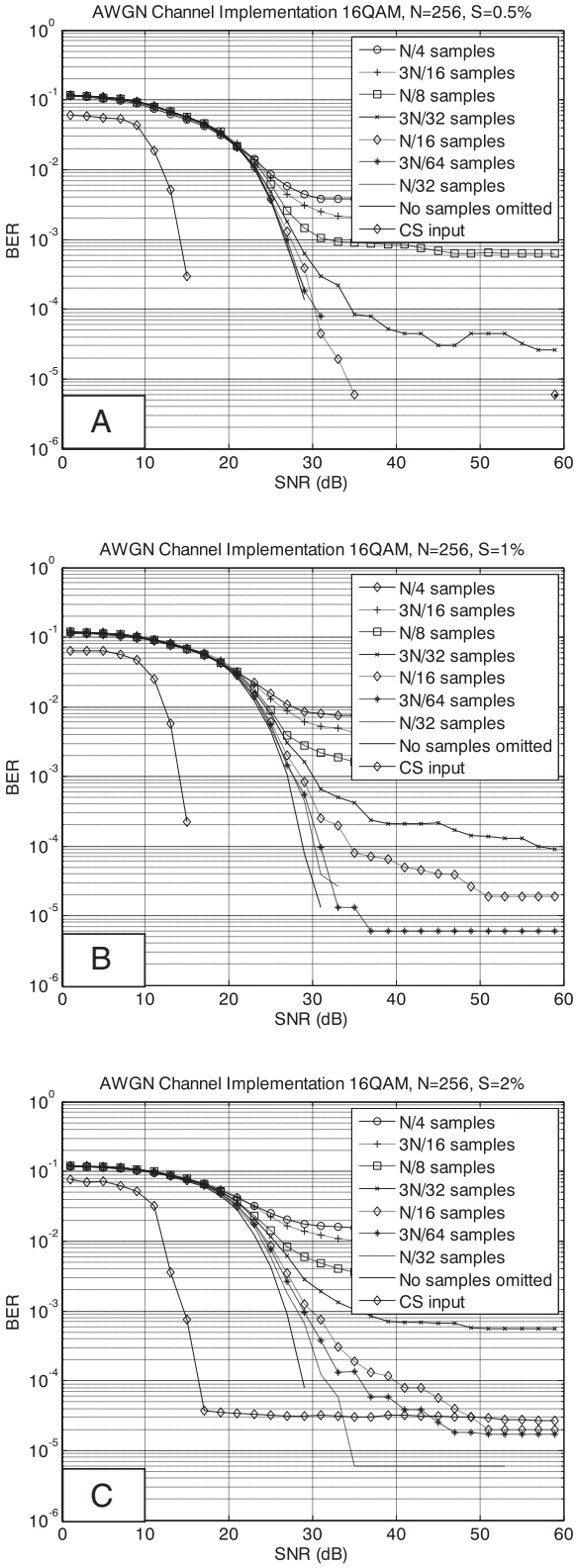

Fig. 7 Simulation Results. Wired OFDM with AWGN channel, $N = 256$ and 16-QAM modulation. **a** Sparseness level $S = 0.5\,\%$, **b** $S = 1\,\%$, **c** $S = 2\,\%$

The STBC-OFMD system described in Section 3.1 is simulated using 16-QAM modulation and $N = 1024$ (Fig. 8). The IFFT input packet structure used, is the one described in Section 3.1 (extension of Fig. 2). This packet structure is appropriate for the normal sub-sampling mode [17]. However, it is also tested for the extended sub-sampling mode that can be applied 75 % of the time. As expected, the BER is worse in Fig. 8 compared to the BER of the wired channel (Figs. 6 and 7). This is owed to the lower wireless channel SNR, the selected QAM modulation order and the size N that is used.

As can be seen from Fig. 8, an error floor always appears but is sufficiently low for several combinations of the parameters that have been taken into account. Specifically, an error floor around 10^{-3} can be achieved, if the number of substituted samples is lower than $R = N/16$.

An image processing example is presented in Fig. 9 in order to visualize the effect of sub-sampling in the STBC-OFDM environment. The original image of the Rio-Antirrio bridge in Greece, as observed in the night from the water level, appears in Fig. 9a. A low noise-high channel SNR of 50 dB was used in order to focus only on the effect of the sub-sampling procedure to the received image. Five different R values were tested and the received images are shown in Fig. 9b–f. The mean square error (MSE) and the normalized MSE (NMSE) of each case is listed in Table 1.

4.2 Discussion-comparison

A brief description of selected referenced approaches follows, along with their experimental or simulation results. The CS approaches are basically used in order to compare their complexity and efficiency with the sub-sampling scheme described in this paper. The comparison is based on the hardware implementation cost, the power consumption, the number of samples used, and the data reconstruction error. The features of the referenced approaches are listed in Table 2. The use of the CS input reference in Figs. 6 and 7 shows that a full signal reconstruction would be possible at a much lower channel SNR. This can be achieved, if the CS measurements are digitized with an adequately high resolution. However, the complexity of the circuits needed for the support of the simulated CS technique would be extremely higher (matrix multiplication, digitization and resolution of the floating point values and measurements, optimization problem solving). The time needed for the reconstruction of a single input would also be considerably higher due to the delay needed for solving the CS optimization problem. Thus, the use of such a CS compression at the input of an OFDM system would not be efficient for real-time applications.

CS techniques have been used for the compression/decompression of a large amount of radar data in

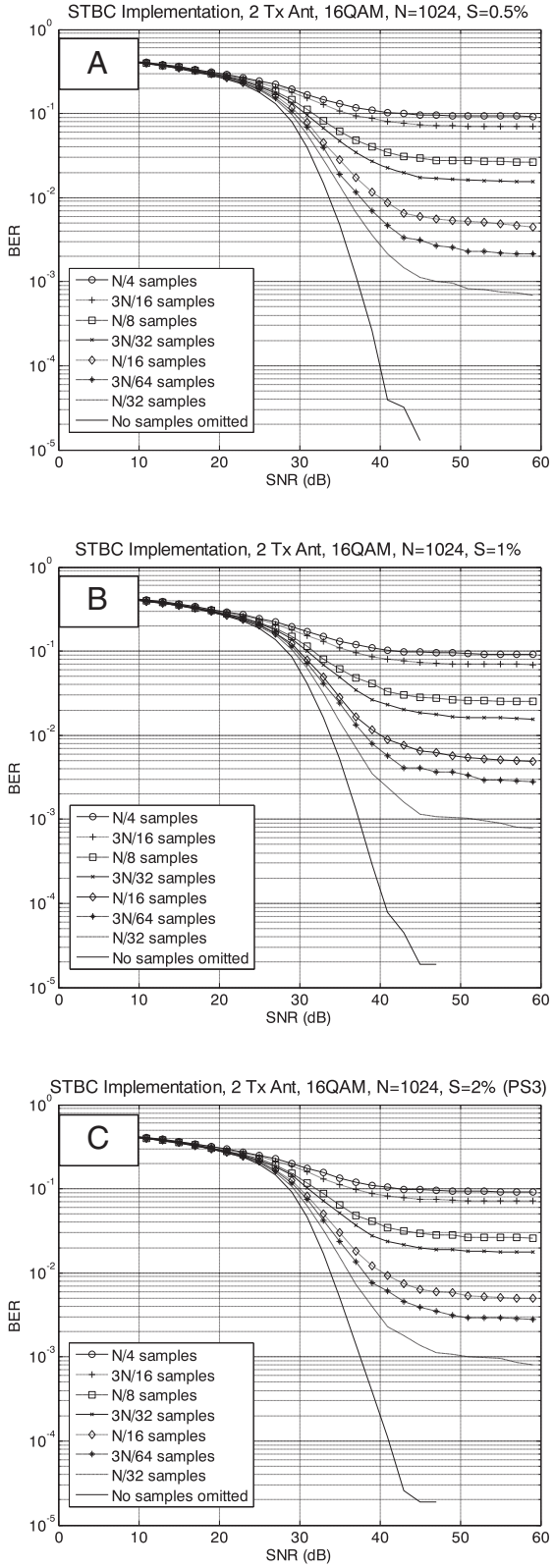

Fig. 8 Simulation results. Wireless STBC-OFDM with 2 transmitters, $N = 1024$ and 16-QAM modulation. **a** Sparseness level $S = 0.5\,\%$, **b** $S = 1\,\%$, **c** $S = 2\,\%$

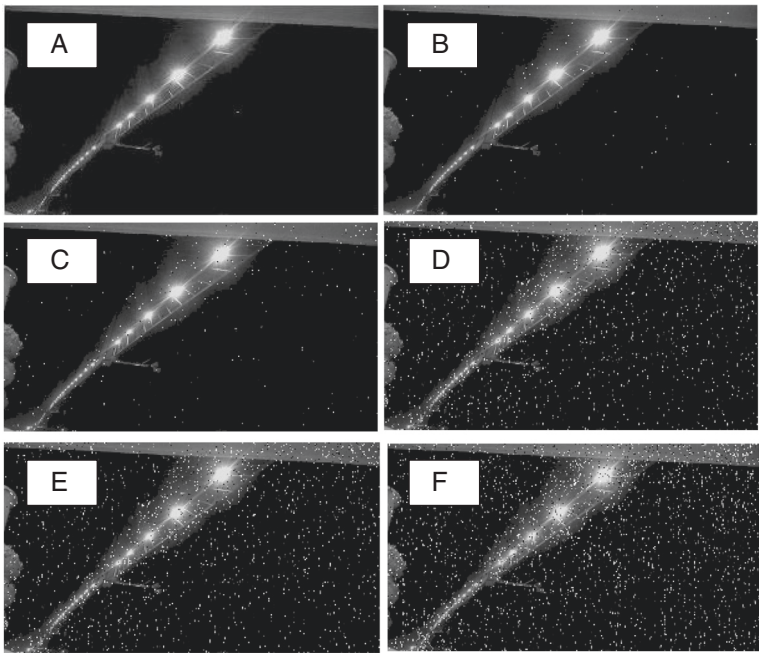

Fig. 9 Image Processing. View of Rio-Antirrio bridge from the sea level. Sparseness $S = 10\,\%$. **a** Original image, **b** reconstructed images with $R = 3N/64$, **c** $R = N/16$, **d** $R = 3N/32$, **e** $R = N/8$, **f** $R = 3N/16$

[4]. NMSE ranges between 1.5 and 3 when fewer measurements are used than the number of sensors otherwise a full reconstruction is possible. A surveillance system is described in [5]. The significant part of the image is lightly compressed, in contrast to the rest of the image that is heavily compressed. A weighted contribution of the signal factors is used in order to focus on the regions of interest. These weights are retrieved either from a Discrete Cosine Transform (DCT), or the Karhunen Loeve (KL) transform of the image coefficients. A comparison is performed with the least angle regression (LARS) algorithm.

The CS model is solved as a Kalman filter in [7] by taking the dual optimization problem. In [8], the proposed approach achieves an NMSE that ranges between 0.02 and 0.1 and increases as the time passes and the error accumulates. In [9], the test error rate is approximately 0.05 when 5 of the 30,000 data bits are non-zero and is increased to 0.075 when 30 bits are different than zero. In the simulation setup of [10], 12 pilots are placed in random 12 of 24 preselected positions in 256 subcarriers. An $NMSE \leq 10^{-5}$ is achieved when SNR is 50 dB.

Table 1 MSE/NMSE for the reconstruction of the images in Fig. 9

Substituted samples	MSE	NMSE
$R = 3N/64$	0.11	0.0019
$R = N/16$	0.3	0.0052
$R = 3N/32$	0.47	0.0081
$R = N/8$	1.6	0.0277
$R = 3N/16$	2.32	0.04

The work presented in [11] can be considered as the most relevant to the proposed sub-sampling method since it concerns compressed data recovery in an OFDM environment. The authors describe a Parallel Segmented Compressed Sensing (PSCS or its extended version EPSCS) architecture where AIC instead of Nyquist sampling is applied. Their target is to use K subcarriers of the 112 offered by the ECMA 368 standard. The BER can fall below 10^{-4}, regardless of the optimization algorithm used provided that: (a) the number of subcarriers K is less than 86, (b) the SNR is higher than 40 dB, and (c) channel estimation is applied.

In [14], an image is used with noise present and SNR = 16 dB. The dimensions of the image used, are $280 \times 280 = 78400$ pixels, with 3509 of them being non-sparse (or equivalently $S = 4.4\,\%$). In [15], a 4×4 MIMO system with 256 subcarriers is simulated and the BER is examined for a different number of active subcarriers (between 4 and 32).

In [25], the BER achieved in systems that use STBC-OFDM coding similar to the one used here (dimensions: 2×2, 16-QAM modulation, Alamouti or Golden encoding), without sub-sampling, is presented and can be used as a reference. Similarly, the symbol error rate (SER) of space time space (3D) MIMO STBC systems with 4 transmit antennas is presented in [26].

Table 2 Main features of the referenced approaches

Reference	NMSE/BER	Notes
This work		In all cases, signal to channel noise ratio>30 dB
	$BER < 10^{-3}$	AWGN, 16-QAM, $N = 256$, $R < N/8$, $S \leq 2\,\%$
	$BER < 10^{-4}$	AWGN, 4-QAM, $N = 1024$, $S \leq 2\,\%$
	$BER < 10^{-3}$	STBC-OFDM, 16-QAM, $N = 1024$, $R < 3N/64$, $S \leq 2\,\%$
	$NMSE < 10^{-2}$	Image of Fig. 7, $R < N/4$, $S = 10\,\%$
This work	$BER < 10^{-4}$	AWGN, 16-QAM, $N = 256$, $S \leq 2\,\%$, $SNR > 17dB$
CS input	$BER < 10^{-2}$	AWGN, 4-QAM, $N = 1024$, $S \leq 2\,\%$, $SNR > 8dB$
[4]	$NMSE < 2.5$	SNR between -5dB and 4dB,
		50 measurements, 100 sensors
	$NMSE > 3$	SNR between -5dB and 4dB,
		20 measurements, 50 sensors
	$NMSE = 0$	$\#measurements > \#sensors$
[5]	$NMSE = 0.18$	Measurements used: 25 %
	$NMSE \approx 0$	Measurements used: 63 %, KL coefficients used
	$NMSE = 0.2$	31.25 % of measurements used with LARS or
		11.72 % used with KL
[7]	MSE=0 to 0.8	e.g., sparseness 4 % or
		10 % (fraction of measurements used)
[8]	$0.02 < NMSE < 0.1$	The proposed approach in [8]
	$0.1 < NMSE < 1$	Compared approaches
[9]	Error Rate:	Sparseness between
	from 0.05 to 0.075	5/30,000 and 30/30,000
[10]	$NMSE < 10^{-5}$	$SNR = 50dB$
[11]	$BER < 10^{-4}$	Subcarriers used:
		≤ 86 ($S = 86/112 \approx 77\,\%$), $SNR > 40dB$
[14]	$NMSE = 0.0085$	$S = 4.4\,\%$, $SNR = 16dB$
[15]		4×4 MIMO, $SNR = 15dB$
	$BER < 10^{-5}$	Active: 4 of 256 subcarriers ($S = 1.56\,\%$)
	$BER > 10^{-2}$	Active: 32 of 256 subcarriers ($S = 12.5\,\%$)
[25]		STBC 2×2-OFDM, 8K carriers,
		no compression/sub-sampling:
	$BER < 10^{-4}$	Depending on: Alamouti or Golden encoding,
		16-QAM or 64-QAM modulation
	$13dB < SNR < 22dB$	equal/unequal transmit power (by 6dB)

Table 2 Main features of the referenced approaches *(Continued)*

Reference	NMSE/BER	Notes
[26]	$SER = 10^{-4}$	3D MIMO
	$@\ SNR = 15dB$	STBC-4 $\times$ 2, 4-QAM
	$SER = 10^{-4}$	3D MIMO
	$@\ SNR = 25dB$	STBC-4 $\times$ 2, 16-QAM

As can be seen from the results listed in Table 2, a BER around 10^{-4} (achieved in many cases in this work when channel SNR is above 30 dB), is acceptable compared either to the reference [25], or the most relevant approaches like [11]. The NMSE can be used as a measure to compare different image processing techniques at least if the images used have a comparable sparseness. The NMSE achieved by the image processing example included in this work is in the same order or better than the NMSE measured in [4, 5, 8, 14]. The required signal to channel noise ratio needed to achieve the results presented here, seems much higher than the one required in many references or the case with the CS input. However, as can be seen by Figs. 6, 7 and 8, an SNR higher than 30dB is needed anyway, for full input recovery in the reference case, where no samples are omitted ($R = 0$).

The obvious advantage of the presented sub-sampling method is its deterministic nature that favours a hardware implementation with very low cost. All the referenced approaches, like compressive sensing and Kalman filters are based on iterative or recursive optimization procedures as explained in detail above. Although the order of the FFT complexity remains $O(N \cdot log_2 N)$, the operations of the FFT are further reduced by 3/8 if $R = N/4$ or 1/8 if $R = N/8$. The complexity of the process needed for the ADC sub-sampling control and the formation of the IFFT input structures is $O(1)$. This is because they require constant time, instead of the additional delay needed by the CS approaches for their optimization problems. A significant power saving can be achieved during the transmission of sparse information due to the reduced sampling rate of the ADC on the receiver side. More specifically, the power consumed by an ADC is proportional to its sampling rate. The memory requirements for sample storage are also reduced as explained in [17] and Section 2.3, and the speed is increased due to the deactivation of large IFFT/FFT sub-blocks.

5 Conclusions

In this paper, a sub-sampling method has been proposed and evaluated for wired OFDM and STBC-OFDM wireless environments. It can be implemented with very low cost hardware in order to reduce the power consumption, the memory requirements and increase the processing speed of an OFDM system. The ADC on the receiver side

can operate in lower sampling rate at up to 3/4 of the time. The deactivation of large IFFT/FFT sub-blocks in the same time interval is feasible. The transmitted information can be fully recovered with small BER (below 10^{-3}), in most of the cases that have been examined. The simulations were performed for combinations of 4-QAM or 16-QAM modulation, 256-pt or 1024-pt FFT and data sparseness between 0.5 and 2 %. An image with 10 % sparseness was also processed in the proposed OFDM environment with NMSE between 0.002 and 0.01.

Future work will focus on the improvement of the proposed sub-sampling technique in order to use fewer samples for the information recovery and achieve a lower error. The proposed OFDM system will also be implemented on real hardware.

Competing interests
The authors declare that they have no competing interests.

Acknowledgements
This work is protected by the provisional patents 1008564 (published September 9, 2015) and 1008130 (published March 6, 2014), Greek Patent Office (OBI).

Received: 5 February 2016 Accepted: 21 April 2016
Published online: 04 May 2016

References

1. EJ Candès, MB Walkin, An introduction to compressive sampling. IEEE Signal Process. Mag. **25**(2), 25–30 (2008)
2. A Kulkarni, H Homayoun, T Mohsenin, in *Proceedings of the 24'th Annual Great Lakes Symposium on VLSI (GLSVLSI'2014), May 21-23, 2014*. A parallel and reconfigurable architecture for efficient omp compressive sensing reconstruction (ACM, Houston, USA, 2014), pp. 299–304
3. YM Tsai, KY Huang, HT Kung, D Vlah, YL Gwon, LG Chen, in *Proceedings of the 2012 Workshop on Signal Processing Systems, 17-19 Oct 2012*. A chip architecture for compressive sensing based detection of ic trojans (IEEE, Quebec, Canada, 2012), pp. 61–66
4. L Xu, Q Liang, in *IEEE ICC 2012 – Ad Hoc and Sensor Networking Symposium, 10-15 June 2012*. Compressive sensing fin radar sensor networks using pulse compression waveforms (IEEE, Ottawa, Canada, 2012), pp. 794–798
5. A Mahalanobis, R Muise, Object specific image reconstruction using a compressive sensing architecture for application in surveillance systems. IEEE Trans. Aerospace Electron. Syst. **45**(3), 1167–1180 (2009)
6. F Fazel, M Fazel, M Stojanovic, Random access compressed sensing of energy-efficient underwater sensor networks. IEEE J. Sel. Areas Commun. **29**(8), 1660–1670 (2011)
7. A Carmi, P Gurfil, D Kanevsky, Methods for sparse signal recovery using Kalman filtering with embedded pseudo-measurement norms and quasi-norms. IEEE Trans. Signal Process. **58**(4), 2405–2409 (2010)
8. H Guo, C Qiu, N Vaswani, An online algorithm for separating sparse and low-dimensional signal sequences from their sum. IEEE Trans. Signal Process. **62**(16), 4284–4297 (2015)
9. J Ziniel, P Schniter, P Sederberg, Binary linear classification and feature selection via generalized approximate message passing. IEEE Trans. Signal Process. **63**(8), 2020–2032 (2015)
10. A Hormati, M Vetterli, Compressive sampling of multiple sparse signals having common support using finite rate of innovation principles. IEEE Signal Process. Lett. **18**(5), 331–334 (2011)
11. T Agrawal, V Lakkundi, A Griffin, P Tsakalides, in *Proceedings of the IEEE Radio and Wireless Symposium (RWS), 16-19 Jan 2011*. Compressed sensing for ofdm uwb systems (IEEE, Phoenix AZ, USA, 2011), pp. 190–193
12. H Hassanieh, P Indyk, D Katabi, E Price, in *Proceedings of the IEEE STOC, 19-22 May 2012*. Near-optimal algorithm for sparse fourier transform (IEEE, New York, USA, 2012), pp. 563–578
13. B Ghazi, H Hassanieh, P Indyk, D Katabi, E Price, L Shi, in *Proceedings of the IEEE Allerton Conference on Communication, Control, and Computing, 2-4 Oct 2013*. Sample-optimal average-case sparse fourier transform in two dimensions (IEEE, Monticello-IL, USA, 2013), pp. 1258–1265
14. S Pawar, K Ramchandran, in *Proceedings of the IEEE International Symposium on Information Theory Proceedings (ISIT), 7-12 July 2013*. Computing a k-sparse n-length discrete fourier transform using at most 4k samples and o(k log k) complexity (IEEE, Istanbul, Turkey, 2013), pp. 464–468
15. J Xu, G Choi, in *Proceedings of the IEEE International Conference on Computing, Networking and Communications (ICNC), 16-19 Feb. 2015*. Compressive sensing and reception for mimo-ofdm based cognitive radio (IEEE, Garden Grove CA, 2015), pp. 884–888
16. Q Zhao, Z Wu, X Li, Energy efficiency of compressed spectrum sensing in wideband cognitive radio networks. EURASIP J. Wireless Commun. Netw. **2016**(83), 1–11 (2016)
17. N Petrellis, Under-sampling in ofdm telecommunication systems. MDPI Appl. Sci. **4**(1), 79–98 (2014)
18. N Petrellis, in *Proceedings of the 19th Panhellenic Conference on Informatics (PCI '15). 1-3 October 2015*. Under-sampling based on sparse data/parity patterns in stbc-ofdm environment (ACM, Athens, Greece, 2015)
19. C Pimentel, R Demo Souza, BF Uchoa-Filho, I Benchimol, in *Proceedings of the International Symposium on Information Theory, 31 Jul-3 Aug 2011*. Minimal trellis for systematic recursive convolutional encoders (IEEE, St. Petersbourg, Russia, 2011)
20. B Widrow, I Kollár, *Quantization noise: roundoff error in digital computation, signal processing, control, and communications*. (Cambridge University Press, Cambridge, UK, 2008)
21. JW Cooley, JW Tukey, An algorithm for the machine calculation of complex fourier series. Math. Comput. **19**, 297–301 (1965)
22. R Lyons, Reducing fft scalloping loss errors without multiplication. IEEE Signal Process. Mag. **28**(2), 112–116 (2011)
23. A Mohammadi, F Ghannouchi, *RF Transceiver Design for MIMO Wireless Communications*. (Springer, UK, 2012)
24. SM Alamouti, A simple transmit diversity scheme for wireless communications. IEEE J. Selected Areas Commun. **16**(8), 1451–1458 (1998)
25. Y Nasser, JF Hélard, M Crussière, in *Proceedings of the International Symposium on Signal Processing Advances in Wireless Communications, 6-8 July 2008*. Bit error rate prediction of coded mimo-ofdm systems (IEEE, Recife, Brasil, 2008), pp. 181–185
26. M Liu, M Crussière, M Hélard, JF Hélard, Achieving low-complexity maximum-likelihood detection for the 3d mimo code. EURASIP J. Wireless Commun. Netw. **2014**(20), 1–16 (2014)